Direct observation of photoinduced bent nitrosyl excited-state complexes

*Karma R. Sawyer, Ryan P. Steele, Elizabeth A. Glascoe[†], James F. Cahoon, Jacob P. Schlegel, Martin Head-Gordon and Charles B. Harris**

Contribution from the Department of Chemistry, University of California, Berkeley, California 94720 and Chemical Science Division, Lawrence Berkeley National Laboratory, Berkeley California 94720.

*cbharris@berkeley.edu

RECEIVED DATE (to be automatically inserted after your manuscript is accepted if required according to the journal that you are submitting your paper to)

[†] present address: Lawrence Livermore National Laboratory, mail stop L-235, 7000 East Ave, Livermore, CA 94550

ABSTRACT.

Ground state structures with side-on nitrosyl (η^2-NO) and isonitrosyl (ON) ligands have been observed in a variety of transition-metal complexes. In contrast, excited state structures with bent-NO ligands have been proposed for years but never directly observed. Here we use picosecond time-resolved infrared spectroscopy and density functional theory (DFT) modeling to study the photochemistry of $Co(CO)_3(NO)$, a model transition-metal–NO compound. Surprisingly, we have observed no evidence for ON and η^2-NO structural isomers, but have observed two bent-NO complexes. DFT modeling of the ground and excited state potentials indicates that the bent-NO complexes correspond to triplet excited states. Photolysis of $Co(CO)_3(NO)$ with a 400-nm pump pulse leads to population of a manifold of excited states which decay to form an excited state triplet bent-NO complex within 1 ps. This structure relaxes to the ground triplet state in ca. 350 ps to form a second bent-NO structure.

KEYWORDS. Transition-metal–nitrosyl complexes, density functional theory, ultrafast spectroscopy, inorganic photochemistry, excited state dynamics, bent-nitrosyl complexes

I. Introduction

The reactivity of transition-metal–NO complexes is different than the reactivity of isoelectronic transition-metal–CO complexes,[1-4] and there is interest in the chemistry of these molecules because NO is an important signaling molecule in biological systems.[2,3] Recent work has shown that irradiation of some transition-metal–NO complexes leads to structural isomers that may be involved in neurotransmission and cancer reduction.[5-7] The photophysical properties of transition-metal–NO complexes, such as $[Fe(CN)_5(NO)]^{2-}$, are also of interest because of long-lived metastable states that are promising for optical data storage.[8-11]

The unusual reactivity of transition-metal–NO complexes is attributed to the unpaired electron on the NO radical.[1,12-17] The NO ligand usually binds to transition-metals with a linear MNO bond angle yet may also bind in a bent geometry (120–170°).[1,4] A shift from a linear to bent geometry is accompanied by a shift in electron spin density from the metal to the NO ligand. This unusual characteristic is regularly cited in inorganic chemistry textbooks and is key to the thermal and photochemical reactivity of transition-metal–NO compounds.[1,18-20] Recent work has also shown that at least 80 transition-metal–NO complexes possess ground state structural isomers with isonitrosyl (M–ON) or side-on nitrosyl ligands (η^2-NO).[9] Figure 1 shows the differences in geometry, back-bonding and M–NO angle between the structures.

Stable transition-metal-NO complexes have either linear- or bent-NO ligands, whereas ON and η^2-NO metastable structures are formed by visible irradiation of stable compounds. The photochemical formation of ON and η^2-NO complexes is well-established.[8-11,21,22] It has also been suggested that visible irradiation of linear-NO complexes leads to the formation of a triplet bent-NO excited state,[23,24] but a bent-NO excited state has never been directly observed.[9] In this study, we use ultrafast time-resolved infrared (IR) spectroscopy to examine the excited state structures and dynamics of a model transition-metal–NO complex, $Co(CO)_3(NO)$. We observe two bent-NO excited state complexes and their dynamics for the first time but find no evidence for either the ON or η^2-NO isomers. We have used density functional theory (DFT) modeling to calculate the structures, frequencies, and energetics of the

ground and excited state complexes. DFT analysis indicates that 400-nm irradiation of $Co(CO)_3(NO)$ leads to the formation of a triplet excited state with a bent-NO ligand which decays in ca. 350 ps to form a bent-NO complex in the ground triplet state. This work provides the first direct evidence for photochemically induced bent-NO transition-metal complexes.

$Co(CO)_3(NO)$, a model transition-metal–NO complex, has a linear Co–NO bond in the electronic ground state (S_0).[4,18,23-25] The electronic absorption spectrum of $Co(CO)_3(NO)$ (Figure 2) shows two bands between 200 and 400 nm. The strong band centered at 200 nm (dissociative band) is assigned to an excitation that leads to cleavage of either the Co–CO or the Co–NO bond.[26] The weak band, centered at 380 nm (σ_{380} = 1.8 x 10^{-18} cm^2), is attributed to a cobalt-to-nitrosyl (Co→NO) charge-transfer transition.[26] Photochemical excitation into this band is proposed to lead to a geometry change to a bent-NO complex.[24] The relatively low intensity of the 380-nm band illustrates that the Co→NO charge-transfer transition is a minor photochemical pathway.[25,27]

The differences between the linear- and bent-NO bonding modes of $Co(CO)_3(NO)$ are shown in the molecular orbital correlation diagram of the $\{CoNO\}^{10}$ structural unit predicted by Enemark and Feltham (Figure 3).[23,24] In the ground electronic state, the HOMO is the $4a_1$ orbital, primarily a cobalt d_{z^2} orbital, and the LUMO is the 4*e* orbital, the totally anti-bonding π-type molecular orbital that is primarily the cobalt d_{xz} and d_{yz} orbitals and the π*(NO) orbitals. Irradiating $Co(CO)_3(NO)$ with 400 nm light corresponds to a $4a_1$→4*e* transition, and upon promoting an electron to the 4*e* orbital, the relative energies of the 4*e* and 3*e* orbitals shift. The molecule then rearranges to lower the orbital energies and forms a triplet complex with a bent Co–NO bond angle. Note that this picture also predicts a change in the geometry of the entire structure from tetrahedral to pseudo-square planar.[24]

Despite the molecular orbital arguments that photolysis of $Co(CO)_3(NO)$ results in the formation of a triplet bent-NO complex, there is debate in the literature regarding this mechanism.[24-29] Gas phase studies suggest that visible photolysis of $Co(CO)_3(NO)$ results in the formation of an excited state of $Co(CO)_3(NO)$ with a bent Co–NO bond and a negatively charged NO ligand.[24] These authors also showed that visible irradiation of $Co(CO)_3(NO)$ in Lewis base solution (e.g.PPh_3, $AsPh_3$ and pyridine)

results in associative photochemical substitution of a single CO, providing indirect evidence for a coordinatively unsaturated bent-NO complex.[24] However, the only photochemical reaction observed via IR studies of $Co(CO)_3(NO)$ in frozen matrices and in the gas phase is the dissociation of a CO or NO ligand.[25,26,29] The goal of this study is to determine whether a bent-NO complex is formed from visible photolysis of $Co(CO)_3(NO)$, and, if it is formed, to determine the mechanism for its formation.

II. Methods

A. Sample Preparation

$Co(CO)_3(NO)$ and spectroscopic grade hexane were purchased from Strem Chemicals Inc. and EMD Chemicals Inc., respectively. All samples were used without further purification. Dilute solutions of $Co(CO)_3(NO)$ in hexane were stable when exposed to air under ambient conditions.

B. Ultrafast Visible-pump, IR-probe Spectroscopy

The setup consists of a Ti:sapphire regenerative amplifier (SpectraPhysics, Spitfire) that is seeded by a Ti:sapphire oscillator (SpectraPhysics, Tsunami) to produce a 1 kHz train of 100 fs pulses centered at 800 nm with an average pulse power of 0.9 mJ. The output of this system is split, and 30% of the output is used to generate 400 nm (1.6 μJ at sample) pump pulses. The remaining 70% is used to pump a homebuilt two-pass BBO based optical parametric amplifier (OPA), the output of which is mixed in a $AgGaS_2$ crystal to produce mid-IR probe pulses tunable from 3.0–6.0 μm with a 200 cm^{-1} spectral width and a ca. 100 fs pulse duration. The 400-nm pulses pass through a 25 cm silica rod, which stretches the pulses in time to 1 ps, and gives a cross correlation of the mid-IR and 400 nm pulses of 1.1 ps at the sample. The stretched 400 nm pulses are necessary in order to achieve high pump powers and low signal-to-noise without generating products due to multi-photon excitation. Further, the stretched pulses prevent artifacts resulting from nonlinear optical effects in the sample cell windows. A high pump power is particularly advantageous here because the Co→NO charge transfer pathway is a minor pathway compared to photodissociation (Figure 2).

The polarization of the 400 nm pump beam with respect to the mid-IR probe beam is held at magic angle (54.7°) to eliminate effects from rotational diffusion. A computer controlled translation stage

(Klinger) allows for variable time delays up to 800 ps between visible-pump and mid-IR-probe pulses. The sample is flowed using a mechanical pump through a stainless steel cell (Harrick Scientific) fitted with 1.5-mm thick CaF_2 windows. The mid-IR probe and 400 nm pump beams are spatially overlapped at the sample and focused so that the beam diameters at the sample are 100 μm and 200 μm respectively. The sample cell is moved by computer controlled translational stages (Standa) after each measured spectrum so that absorptions are not altered because of photoproduct accumulating on the sample cell windows. Reference and signal mid-IR beams are sent along a parallel path through a computer controlled spectrograph with entrance slits set at 35 μm (Acton Research Corporation, SpectraPro-150) and detected by a 2x32 element MCT-array IR detector (InfraRed Associates, Inc.) and a high-speed signal acquisition system and data acquisition software (Infrared Systems Development Corp.) with a resolution of ca. 3 cm^{-1}. Collected signals are averaged over 1000 laser shots to correct for shot-to-shot fluctuations. Differences in optical density (ΔOD) as small as $5x10^{-5}$ are observable after one second of data collection.

Kinetic data presented in this work result from spectra measured at time delays between 1 and 800 ps between the visible pump and mid-IR probe pulses. For each spectral feature, the kinetic data were determined by plotting the peak intensity at a single wavenumber as a function of delay time. The kinetic data were fit to sums of exponentials, convoluted with a Gaussian (FWHM = 1.1 ps) in order to accurately reflect the instrument response time using the Levenberg-Marquart method. All of the errors in the kinetic data are reported at 95% confidence intervals.

C. Density Functional Theory Modeling

Kohn-Sham Density Functional Theory (DFT)[30] calculations were performed with a development version of Q-Chem 3.1.[31] The BP86 functional[32,33] was employed, as it generally gives satisfactory results for transition-metal systems.[34] The agreement between the calculated NO stretching frequency for $Co(CO)_3(NO)$ (1842 cm^{-1}) is in reasonable agreement with the known experimental values (1808 cm^{-1}) and is typical of the observed accuracy for this functional.[35,36] Furthermore, our initial tests verified that the calculations adequately predict vibrational frequencies for $Co(CO)_3(NO)$ without

empirical scaling.[34,36] An analysis of basis set and functional dependence of frequencies is provided in the SI. All calculations are reported using the 6-311+G(3df)[37-39] basis set for the ligands and 6-31G* for the metal center. Cartesian *d* functions were used for both basis sets. Though the 6-311G basis does not exist for Co, further extension of the basis set to cc-pVTZ[40,41] produced only marginal (1–9 cm^{-1}) changes in reported frequencies, at significantly increased computational expense. No pseudopotentials were employed for the metal center. Initial testing indicated that a pseudopotential (LANL2DZ)[42] led to relatively insignificant (≤5 cm^{-1}) changes in the CO and NO stretching frequencies. Additionally, omitting the core potential simplified analysis of basis set effects. All calculations were performed with the SG-1 integration grid.[43] The self-consistent field was converged to 10^{-8} a.u., using integral thresholds of 10^{-12} a.u. Geometry optimizations were converged to the Q-Chem default tolerances of $3x10^{-4}$ a.u. (max gradient) and either $12x10^{-4}$ a.u. (displacement) or $1x10^{-6}$ a.u. (energy). No symmetry constraints were applied, and initial structures were perturbed to check for structures of lower symmetry.

Excited state single-point energies were obtained with time-dependent DFT (TD-DFT)[44-47] within the Tamm-Dancoff approximation,[48] using the parameters described above. The structure and frequency of the first excited singlet (S_1) were obtained with a spin-corrected single-reference method using the Maximum Overlap Method to produce the excited configuration.[49] Further details may be found in the Supporting Information (SI).

III. Results and Discussion

A. Ultrafast visible-pump, IR-probe spectroscopy of $Co(CO)_3(NO)$ in neat solution

Figure 4 shows the ultrafast visible-pump, IR-probe spectra of $Co(CO)_3(NO)$ (**A**) in neat hexane solution, and the dynamics and peak assignments of the features are listed in Table 1. Peak assignments are based on the observed kinetics and peak positions and the DFT analysis discussed in below. Figure 4a-4b show peaks in the NO stretching region, and Figure 4c shows peaks in the CO stretching region. Features attributed to parent molecules (**A**) (1807, 2037 and 2100 cm^{-1}) and $^1Co(CO)_2(NO)$(hexane) and $Co(CO)_3$, are not shown here for clarity but are presented in the SI.[25,29,50]

The spectra in Figure 4 show peaks that are not attributable to either of the CO- or NO-loss pathways that have been observed in past studies,[25,29] confirming that there are intermediates formed via non-dissociative photochemical pathways. The experimental results for these pathways are discussed herein. Figures 4a and 4b show peaks centered at 1684, 1715, and 1755 cm^{-1}, respectively. The relatively low stretching frequencies of the peaks indicate that they correspond to NO stretching modes. The DFT calculations presented in section III B indicate that CO ligands of all of the possible intermediates are terminally bound, and consequently, it is unlikely that their stretching frequencies will be more than 100 cm^{-1} lower than the asymmetric CO stretch of **A** (2037 cm^{-1}).[51-54] This is further supported by past studies,[25,26,29] which indicate that none of the CO- and NO-loss intermediates possess a CO stretching mode below ca. 1980 cm^{-1}. Thus, we assign the 1684, 1715, and 1755 cm^{-1} peaks (labeled $\mathbf{C_{NO}}$, $\mathbf{B_{NO}}$, $\mathbf{D_{NO}}$) to the stretching frequency of the NO ligand in three distinct complexes, **C**, **B** and **D**.

The peak labeled $\mathbf{D_{NO}}$ partially decays with a time constant of $\tau = 11 \pm 1$ ps (Table 1) and is stable for the duration of the experiment. The fast decay of this peak is similar to the recovery of the NO stretch of **A** (23 ± 1 ps) and the decay of the NO stretch of the vibrationally hot parent molecules (17 ± 2 ps) (refer to SI). Therefore, the decay of $\mathbf{D_{NO}}$ is assigned to vibrational cooling of the NO ligand and not to CO loss reactive dynamics. The peaks labeled $\mathbf{B_{NO}}$ and $\mathbf{C_{NO}}$ do have dynamics that are separate from vibrational cooling. Neglecting the vibrational cooling dynamics, the $\mathbf{B_{NO}}$ peak decays with a time constant of $\tau = 359 \pm 150$ ps and $\mathbf{C_{NO}}$ rises with a time constant of $\tau = 350 \pm 100$ ps (Figure 5). The agreement of the time constants suggest that species **B** converts to species **C** in approximately 350 ps.

Figure 4c shows two peaks centered at 1913 and 1949 cm^{-1}. Neglecting vibrational cooling dynamics, exponential fits to these peaks yield a decay time of 209 ± 78 ps and a rise time of 297 ± 18 ps, respectively (Figure 6). Since these time constants are similar to the time constants obtained for peaks $\mathbf{B_{NO}}$ and $\mathbf{C_{NO}}$, we propose that they correspond to the CO stretching modes of species **B** and **C**.[51-54] The CO stretching frequencies of species **D** ($\mathbf{D_{CO}}$) were not observed experimentally, most likely because the CO stretch of **D** was hidden by the larger peaks from the CO- and NO-loss pathways.

The shifts in the frequency of the $\mathbf{B_{NO}}$, $\mathbf{C_{NO}}$ and $\mathbf{D_{NO}}$ peaks relative to the NO stretch of **A** provide clues to their structures.[1,4,9] Within a given complex, the stretching frequencies of the bent-NO, ON and η^2-NO ligands are red-shifted relative to the stretching frequency of the linear-NO ligand. The η^2-NO stretching mode is generally ca. 400 cm^{-1} lower in energy than the linear-NO mode (1807 cm^{-1} for **A**).[25] Consequently, if a complex with an η^2-NO ligand was formed from visible irradiation of $Co(CO)_3(NO)$, we would not be able to observe the η^2-NO stretch because our experimental setup does not permit us to monitor absorptions below 1650 cm^{-1}. Similarly, an ON stretching mode is generally ca. 100 cm^{-1} lower in energy than the corresponding linear-NO mode.[9,55] However, we do not expect to observe an ON complex since past studies indicate that they are typically formed via multi-photon processes.[21,22,55] The stretching frequency of bent-NO ligands is also approximately 100 cm^{-1} lower in energy than the frequency of linear-NO stretches. Linear-to-bent NO conversion can be thought of as rehybridization of nitrogen from sp to sp^2, corresponding to a weakening of the NO bond, thus decreasing the frequency of the NO stretch.[1,4,18,19,24]

Species **B**, **C**, and **D** have lower energy stretching frequencies than species **A** by 92, 113, and 52 cm^{-1}, respectively. Thus, any of these species could correspond to either a complex with an ON or a bent-NO ligand.[4,9] Since none of these species have been observed in past studies, we have utilized DFT quantum chemical modeling to determine their structures, electronic states, energies, and harmonic frequencies.

B. Density Functional Theory Modeling

DFT calculations were used to identify species **B**, **C**, and **D**, and to determine the mechanism that was observed experimentally. The analysis presented herein focuses on static structures and the topography of relevant potential energy surfaces. An explicit, time-dependent simulation of the excited state dynamics following photoexcitation is not feasible because the dynamics are relatively slow (pico- through early nanosecond time scales) and involve multiple excited states. Furthermore, some of the key processes are spin-forbidden, and an explicit simulation would require the calculation of spin-orbit coupling[56,57] to an accuracy commensurate with the energies and couplings. Relevant potential energy surfaces will be used to offer qualitative arguments for the dynamics of the system. The resulting

picture, when compared to the experimental results presented above, lends considerable insight to the photochemical mechanism.

Molecular orbital diagram of $Co(CO)_3(NO)$

Figure 7 shows a partial Kohn-Sham orbital diagram for **A**. It has a linear NO group and a tetrahedral (C_{3v}) geometry, as expected. Both the HOMO and LUMO of **A** are of *e* symmetry and doubly degenerate. The HOMO contains contributions from the overlap of metal d_{xz}/d_{yz} orbitals with π*(NO) orbitals, whereas the LUMO is primarily composed of π*(NO) ligand orbitals. Note that the HOMO-LUMO gap (68 kcal/mol) almost perfectly matches the energy of the 400-nm pump pulse used in the experiment (400 nm ≈ 71 kcal/mol). It is possible that a 400 nm excitation corresponds to the $2a_1 \rightarrow 4e$ electronic transition; DFT predicts that these orbitals are 76 kcal/mol apart (~ 375 nm). However, the TD-DFT calculations presented below show that, while both transitions are weak, the transition moment for the $2a_1 \rightarrow 4e$ transition is ca. half as intense as the transition moment for the $3e \rightarrow 4e$ transition. Ultimately, we expect that both transitions will result in the same dynamics on the picosecond time-scale, provided that the former transition is not dissociative. Note that this diagram is different from the MO diagram in Figure 3, since DFT predicts the a_1 orbital is 8.2 kcal/mol below the HOMO.[23]

The two pairs of degenerate frontier orbitals lead to four single-excitation excited states, discussed further below. Figure 8 shows that as the Co–N–O angle decreases into Cs symmetry, the 3e and 4e orbitals split into non-degenerate pairs, labeled a' and a''. In this staggered geometry the three CO groups are not arranged symmetrically; the angle between two of the CO ligands is slightly wider, creating a gap into which the NO can bend. Optimization of a structure in which the NO bends into the smaller gap between CO ligands was attempted but was unsuccessful as this structure is simply a distorted form of the structure in which the NO is bent into the larger gap. The convention throughout this work is that the positive bending coordinate signifies an NO that is bent so that it bisects the angle between the neighboring CO ligands and the negative bending coordinate denotes an NO ligand bent directly toward the third CO. The *a'* orbital stemming from the original *3e* HOMO (blue) rises in energy, due to diminished π back-bonding. The *a'* and *a''* orbitals stemming from the LUMO (red)

decrease in energy as the Co–N–O angle decreases, suggesting that the lowest-lying singlet and triplet excited states (S_1 and T_1) will have distinctly different structures than the ground state (S_0).

Structures & Harmonic Frequencies

Optimized molecular structures and harmonic frequencies were obtained for structural isomers of the parent compound (**A**) on the ground state potential, the lowest energy structures on the lowest-lying triplet (T_1) and singlet (S_1) excited state potentials, and the singlet and triplet CO-loss complexes. Figure 9 shows the optimized molecular geometries, and the key structural parameters, harmonic frequencies, and relative energies are listed in Table 2.

CO-loss structures

Past studies have indicated that the most significant pathway upon 400 nm photolysis of $Co(CO)_3(NO)$ is CO dissociation.[25,26,29] $^1Co(CO)_2(NO)(S)$ (S = hexane) was observed in the experiments discussed above (ν(NO) = 1775 cm^{-1}).[25,26,29] DFT predicts that the NO ligand is slightly bent (Table 2, Figure 9), and has a stretching frequency (1803 cm^{-1}) that is only 39 cm^{-1} lower in energy than the NO stretch of S_0.[58] In addition to $^1Co(CO)_2(NO)(S)$, a triplet CO-loss complex, $^3Co(CO)_2(NO)$, is accessible with a 400 nm photon.[59] DFT predicts that $^3Co(CO)_2(NO)$ has a linear NO ligand (Figure 8), and a stretching frequency of 1773 cm^{-1}. Peak **D**, which shows no reactive dynamics on the time scale of the experiment, is assigned to be $^3Co(CO)_2NO$ since the calculated frequency agrees well with the **D** peak (1755 cm^{-1}).[60] Furthermore, the singlet–triplet gap (20 kcal/mol)[61] for the CO-loss complexes is large enough that coupling between the states should be small so that $^3Co(CO)_2(NO)$ is long-lived.[62-64]

Ground State Structural Isomers and Lowest Excited State Structures

Figure 9 shows the optimized geometries of the three ground state structural isomers—linear-NO, η^2-NO and ON complexes[65] hereafter referred to as S_0, η^2-S_0, and iso-S_0, respectively. Both S_0 and iso-S_0 contain a linear (iso)nitrosyl group, whereas the Co–NO bond angle in the η^2-S_0 complex is strongly bent (85°) so that it bisects two of the CO ligands. The iso-S_0 and η^2-S_0 structures are 42.0 and 38.4

kcal/mol higher in energy than S_0. The NO stretching frequencies of both isomers are red-shifted from the corresponding stretch of S_0: ν(NO) = 1509 cm^{-1} for η^2-S_0 and 1770 cm^{-1} for iso-S_0.

Figure 9 also shows the optimized molecular structures on the first excited triplet and singlet potentials (T_1 and S_1). Both T_1 and S_1 have bent-NO ligands, with bond angles of 137º and 129º, respectively. Once again, the bond is bent so that it bisects two of the CO ligands, resulting in a pseudo-tetrahedral C_s structure.[23,66] Both of the structures have NO bond lengths that are more than 0.02Å longer than the NO bond in S_0 due to the decrease in the bond order. Additionally, the Co–N bonds are longer by 0.15Å (T_1) and 0.17Å (S_1), due to reduced back-bonding.[67] Accordingly, the NO stretching frequency of the T_1 and S_1 structures are red-shifted relative to S_0: ν(NO) = 1664 cm^{-1} for T_1 and 1659 cm^{-1} for S_1. The calculated NO stretching frequencies for these complexes reflect the differences in their geometries. The red-shifting of the NO stretching modes of the bent-NO ligands confirms that the NO bond is weaker when bound to the metal center in a bent configuration compared to a linear configuration.[67]

The DFT calculations indicate that our experimentally observed peaks cannot be assigned to η^2-S_0 because the frequency of its NO stretch is outside of the experimentally observable range, however, we cannot rule out the possibility that this η^2-S_0 isomer is formed by the pump pulse. Since the calculated NO modes of the iso-S_0, S_1 and T_1 structures are all within error of the experimentally observed peaks, they are all candidates for both **B** and **C**. The calculated frequencies do not provide any information about the dynamics of these complexes; their energies and the barriers connecting them provide the crucial remaining evidence.

Potential Energy Surfaces

One-dimensional slices of the ground and two lowest excited potential energy surfaces (S_0, T_1, and S_1) of $Co(CO)_3(NO)$ were calculated to aid in the identification of **B** and **C**. Since the Co–N–O bond angle appears roughly to be the relevant reaction coordinate, a constrained potential energy scan was calculated while fixing this parameter at successive bond angles ranging between 80º and 180º. The

remaining 3N-7 degrees of freedom were fully optimized at each point. The results of these calculations are presented in Figure 10a.

Ground and Lowest Excited State Potential Energy Surfaces

Figure 10a confirms that the global minimum on the S_0 potential has a linear-NO structure and predicts that a ca. 28 kcal/mol barrier connects S_0 to η^2-S_0. The reverse barrier is only ca. 3 kcal/mol, suggesting that even if η^2-S_0 were formed, it would quickly isomerize back to S_0.[8,68] Iso-S_0 is less stable than S_1 and T_1 (Table 2) and a significant barrier exists to accessing it from either state (refer to SI). Thus, neither **B** nor **C** is due to iso-S_0. This is consistent with previous studies that have shown that multiple photons are needed to form iso-S_0 from S_0 and that the formation of iso-S_0 relies upon the presence of a stable, photochemically accessible η^2-S_0 intermediate.[8,21,22]

Since neither species **B** nor **C** can be assigned to η^2-S_0 or iso-S_0, the unassigned peaks must be due to excited state bent-NO complexes. The calculated NO stretching frequencies for both T_1 (1664 cm^{-1}) and S_1 (1659 cm^{-1}) agree best with the NO stretching mode of **C** (1685 cm^{-1}). Anharmonic corrections to the T_1 frequency via vibrational perturbation theory[69] bring the calculated frequency to 1692 cm^{-1}, even closer to the observed value.

Since the calculated NO stretching frequencies of S_1 and T_1 are indistinguishable given the accuracy of DFT calculations,[36] we have used the calculated potentials in Figures 10b and 10c to further differentiate between them. Figures 10b and 10c show the "vertical" energies of S_0, single-point energy calculations that were performed at the optimized structures of the paired *opt* state. Figure 10c shows that S_1 and S_0 are close in energy in the vicinity of the minimum on the S_1 potential.[11,70,71] We estimate that there is a ca. 2 kcal/mol energetic barrier to accessing the point of closest approach from the minimum energy structure of S_1. However, in the case of the $S_1 \rightarrow S_0$ transition, the coupling between the states is strong and thus the nonadiabatic transition may occur before the classical barrier is crossed.[72] Therefore, S_1 must be short-lived (i.e. less than 1 ps) and cannot be assigned to **C**, which exists for at least 700 ps.

Figure 10b shows also shows a close approach between T_1 and S_0 along the Co–N–O angle. However, because T_1 is a high-spin state, it is reasonable that it is long-lived. The magnitude of spin-orbit coupling in this vicinity—not calculated for these species but typically on the order of 20-200 cm^{-1}—would lower the nonadiabatic transition probability for $T_1 \rightarrow S_0$ transition as compared to the $S_1 \rightarrow S_0$ transition.[62,73,74] Further, there is a small classical barrier (~3 kcal/mol) to accessing the point of closest approach between T_1 and S_0 from the minimum energy T_1 structure, akin to the inverted region of Marcus theory.[75,76] In other words, because the $T_1 \rightarrow S_0$ transition is spin-forbidden, the coupling between the states is weak in all regions except for the crossing point between the states. Thus, *before* the system can undergo the nonadiabatic transition to ground state, it must pass over the classical barrier to access the crossing point.[75,76] As a result, it is reasonable to expect the bent-NO complex in the T_1 to be long-lived. Moreover, since T_1 is a coordinatively unsaturated species in the ground triplet state, it is expected to be unreactive on the picosecond time scale when in solution with saturated alkanes.[62,64,77,78] Since the calculated NO stretching frequency of T_1 is in good agreement with the experimentally observed **C** peak and since the calculated potentials suggest that T_1 would be a stable on the picosecond time scale, we assign species **C** to the bent-NO complex in the ground triplet state, T_1.

Higher Excited State Potential Energy Surfaces

The identification of the short-lived species, **B**, remains. Given that the NO stretch of **B** is red-shifted relative to **A** and slightly blue-shifted relative to **C**, we expect that **B** should be assigned to a complex with a NO ligand that is "less bent" than the NO ligand in **C**. The S_1 complex has a bent-NO ligand, but the S_1 NO stretch is slightly red-shifted, not blue-shifted, from the corresponding mode of **C**. Further, the nonadiabatic $S_1 \rightarrow S_0$ transition is also more plausible than the spin-forbidden $S_1 \rightarrow T_1$ transition, so that if the bent-NO S_1 complex were formed, it would quickly isomerize to the parent rather than decaying to form **C** (T_1).

Since no evidence exists for a bent-NO complex that is less bent than **C** on the ground state (S_0) or either of the two lowest excited states (S_1 or T_1), we expect that **B** corresponds to a complex on a higher excited state. We expect that **B** corresponds to an excited state complex that decays to form T_1 with a

time constant of 350 ps that is either due to a classical barrier or due to low nonadiabatic coupling between the states. To further explore this possibility, we have plotted TD-DFT vertical excitation energies of the higher excited singlet and triplet states along the 588 cm^{-1} NO bending mode (the same coordinate as Figure 8). Figure 11 shows four states that arise from the original, doubly degenerate HOMO and LUMO of **A**. The singlet states are shown in green (circles), and the triplet states are shown in red (triangles). As mentioned earlier, the positive bending mode (right side of Figure 11), the NO ligand bends so that it bisects two of the CO ligands, whereas in the negative bending mode (left side), the structure is eclipsed so that the NO is bent directly towards the remaining CO group. Optimization of these states would lead to more pronounced minima and shift of the Co–N–O angle, as has been observed for T_1 and S_1. All but one of the states in Figure 11 have at least one local minimum that corresponds to a structure with a bent-NO group, and all of the bent-NO structures on the higher states have NO ligands that are less bent than T_1 (**C**).[79] Therefore, based on the bond angles alone, we cannot determine which of the higher excited states corresponds to **B**.

The relative energies and topographies of the excited states in Figure 11 provide the additional information necessary to identify **B**. Three singlet states labeled S_1, S_2 and S_3 are in the vicinity of the photon energy shown in Figure 11 (dashed line at 71 kcal/mol). TD-DFT calculated transition dipole moments predict that only the degenerate S_1 and S_3 states have non-zero oscillator strengths, suggesting that 400-nm photolysis leads to the population of these states, both of which have minimum energy structures with bent-NO ligands. However, all of the singlet excited states with bent-NO ligands intersect with another excited state, typically in the vicinity of local minima. As a result, any population in the excited singlet states will rapidly relax to the lowest energy singlet state, S_0. These dynamics are all expected to occur more quickly than we can observe experimentally;[80] thus, none of the excited singlet states are expected to be involved in the experimentally observed dynamics. It is possible that this pathway occurs and may contribute to the low quantum yield of the pathway involved in the formation of **B** and **C**.

The topography of the excited triplet states is quite different and suggests that **B** corresponds to either the T_2 or T_3 excited triplet states in Figure 11. A relatively large energy gap separates the ground triplet state (T_1) and the higher triplet states (T_2 and T_3), suggesting that the higher triplet states will be relatively long-lived. The point of closest approach between T_1 and the higher triplet states (T_2 and T_3) along this coordinate occurs when the Co–N–O bond is bent into an eclipsed structure, at which point T_1 is ca. 5 kcal/mol lower in energy than the higher states. Significant distortion of this structure would be required for favorable coupling to T_1. Since the staggered and eclipsed minima in the T_2 state and the eclipsed T_3 minimum are nearly isoenergetic and connected by small barriers (ca. 3 kcal/mol), we cannot determine which structure (staggered or eclipsed) or which electronic state (T_2 or T_3) corresponds to **B**. Intuitively, one would expect that the eclipsed structure would be more stable. However, since we cannot perform a full optimization, we cannot rigorously rule out the possibility that **B** corresponds to the staggered structure. A reasonable conjecture is that the excited state structure would have to access the small, but non-zero, barrier connecting the staggered and eclipsed structures in Figure 11 multiple times before transition to T_1 occurs. In other words, the molecule may switch back and forth between the staggered and eclipsed structures on either the T_2 and the T_3 surfaces before relaxing to T_1. While some ambiguity remains in assigning **B** to either T_2 or T_3,[81] it is clear from our analysis that **B** is an excited state triplet complex with a bent-NO ligand. Species **B** is stable for ca. 350 ps before relaxing to form species **C**, a bent-NO complex in the ground triplet state (T_1).

IV. Discussion and Conclusions

Using time-resolved infrared spectroscopy and DFT modeling we have, for the first time, directly observed a photoinduced linear-to-bent NO geometry change in a transition-metal complex. Excited states with bent-NO ligands in transition-metal–NO complexes have been proposed in the literature for 40 years, but the formation of these excited states has never been directly observed.[23-28] We have observed two kinetically correlated, excited triplet bent-NO complexes that exist on the picosecond time scale. We propose the mechanism shown in Figure 12 for the photochemical formation of these bent-NO complexes. Photolysis of $Co(CO)_3(NO)$ with a single pulse of 400-nm light leads to population of a

manifold of short-lived excited states which decay to an excited triplet state (either T_2 or T_3 in Figure 11) in less than one picosecond. The excited triplet structure has a bent NO ligand with a Co–N–O bond angle predicted to be roughly 155°–166°.[82] This structure is stable for 350 ps before nonadiabatic coupling induces a transition to the ground triplet state (T_1). The most stable structure in T_1 also has a bent NO ligand with a Co–N–O bond angle of 137°. The bent-NO complex in T_1 is observable throughout the remainder of our experiment. T_1 is expected to ultimately decay back to the parent, but we do not observe these dynamics on the picosecond time scale.

The UV-visible absorption spectrum in Figure 2 indicates that the formation of the bent-NO complexes is a minor photochemical pathway,[25,27] which is further verified by the low intensity of the $\mathbf{B_{NO}}$ and $\mathbf{C_{NO}}$ peaks in Figure 4. We expect that the triplet bent-NO complexes were not observed in past studies of $Co(CO)_3(NO)$ because the quantum yield for this pathway is so low.[25] It is possible that this pathway is more significant in other systems, but since the bent-NO complexes are excited state structures, they may be too short-lived to be observed by conventional methods.[80] Further experimental and theoretical investigations are suggested to determine the generality of this mechanism and to determine the effect that this pathway has on the photophysical properties of other transition-metal–NO compounds.

Questions remain concerning the generality of this mechanism. Numerous studies have proposed that $[Fe(CN)_5(NO)]^{2-}$ is particularly promising for optical data storage because visible photolysis of this compound leads to formation of Fe-ON and Fe-η^2-NO metastable states. The photochemical formation of these metastable states is extremely common in transition-metal–nitrosyl complexes; it has been observed in 80 compounds, including $Na_2[Fe(CN)_5(NO)]$, Cp*NiNO, $K_2[RuCl_5NO]$ and $[CpRe(CO)_2(NO)]BF_4$.[8,9,11] However, the work presented herein indicates that there are additional photochemical pathways that may decrease the quantum yield for forming the metastable states. Previous studies have ruled out stable triplet states with bent-NO ligands using ESR spectroscopy of complexes such as $[Fe(CN)_5(NO)]^{2-}$ and Cp*Ni(NO).[11] There are two possible reasons why the bent-NO complexes were not observed in those studies: (1) the excited state complexes are too short lived or (2)

the T_1 bent-NO complex is formed in low yield. Even if the latter option is true, any small loss to T_1 may hold significant consequences for accurate and reliable data storage.

In addition, there is interest in transition-metal–NO complexes because they are important in medical applications that rely on the controlled release of NO from metal complexes.[2,3,5-7] The η^2-NO and ON structural isomers are proposed to be important to these processes because the metal-NO bond is weaker in these structures compared to complexes with linear-NO ligands.[6] Similarly, the metal–NO bond is weaker in bent-NO complexes compared to linear-NO structures.[1] Our work suggests that bent-NO complexes may also be used to control NO signaling in biological systems. However, this study is the first to report the photochemical formation bent-NO complexes, and it is still unclear if there are similar mechanisms for more biologically relevant transition-metal–NO complexes.

ACKNOWLEDGMENT

The National Science Foundation Division of Physical Chemistry is acknowledged for funding. We also acknowledge the Office of Basic Energy Sciences, Chemical Sciences Division, of the U.S. Department of Energy under contract DE-AC02-05CH11231 for the use of some specialized equipment and contractor supported research (CSR). R.P.S. acknowledges funding from the National Science foundation under Grant No. CHE-0535710. Special thanks to Renee Frontiera and Prof. Rich Mathies for use of the UV-Vis spectrometer and Aram Yang for helpful discussions.

SUPPORTING INFORMATION PARAGRAPH.

Supporting information includes the following: (1) full spectra of $Co(CO)_3(NO)$ in solution from 1650 and 2100 cm^{-1} including peak assignments for all observed features based on DFT calculated CO and NO stretching modes, (2) discussion of experimental artifact in Figure 4, (3) details about the spin-corrected method used to determine the structure and frequency of S_1, (4) Kohn-Sham orbital diagram of bent-NO complex on T_1 (**C**), (5) ground state potential energy surfaces calculated with fixed Co–N–O bond angles ranging from 0^o to 180^o, (6) TD-DFT excitation energies along the Co-N-O angle, (7)

analysis of basis set and functional dependence of relevant DFT frequencies, (8) Cartesian coordinates of optimized structures. This material is available free of charge via the Internet at http://pubs.acs.org.

References

1. Crabtree, R.H., *The Organometallic Chemistry of Transition Metals*, John Wiley & Sons: New York, NY, 2001; pp. 88-91.

2. Hayton, T.W., P. Legzdins, and W.B. Sharp, *Chemical Reviews* **2002**. 102, 935-991.

3. McCleverty, J.A., *Chemical Reviews* **2004**. 104, 403-418.

4. Richter-Addo, G.B. and P. Legzdins, *Metal Nitrosyls*, Oxford University Press Inc.: New York, 1992; pp.

5. Culoota, E. and D.E. Koshland, *Science* **1992**. 259,

6. Schaniel, D., T. Woike, B. Delley, D. Biner, K.W. Kramer, and H.U. Gudel, *Physical Chemistry Chemical Physics* **2007**. 9, 5149-5157.

7. Stamler, J.S., D.J. Singlet, and J. Loscalzo, *Science* **1992**. 258, 1898.

8. Atanasov, M. and T. Schonherr, *Journal of Molecular Structure* **2002**. 592, 79-93.

9. Bitterwolf, T.E., *Coordination Chemistry Reviews* **2006**. 250, 1196-1207.

10. Boulet, P., H. Chermette, and J. Weber, *Inorganic Chemistry* **2001**. 40, 7032-7039.

11. Coppens, P., D.V. Fomitchev, M.D. Carducci, and K. Culp, *Journal of the Chemical Society Dalton Transactions* **1998**. 865-872.

12. Ford, P.C. and I.M. Lorkovic, *Chemical Reviews* **2002**. 102, 993-1017.

13. Laverman, L.E., A. Wanat, J. Oszajca, G. Stochel, P.C. Ford, and R. van Eldik, *Journal of the American Chemical Society* **2001**. 123, 285-293.

14. Lim, M.D., I.M. Lorkovic, and P.C. Ford, *J Inorg Biochem* **2005**. 99, 151-165.

15. Lim, M.D., I.M. Lorkovic, K. Wedeking, A.W. Zanella, C.F. Works, S.M. Massick, and P.C. Ford, *Journal of the American Chemical Society* **2002**. 124, 9737-9743.

16. Snyder, S.H. and D.S. Bredt, *Sci Am* **1992**. 266, 68.

17. Weichsel, A., J.F. Andersen, S.A. Roberts, and W.R. Montfort, *Nat Struct Biol* **2000**. 7, 551-554.

18. Geoffroy, G.L. and M.S. Wrighton, *Organometallic Photochemistry*, Academic Press: New York, 1979; pp. 134-135; 157-160.

19. Huheey, J.E., E.A. Keiter, and R.L. Keiter, *Inorganic Chemistry: Principles of Structure and Reactivity*, Harper Collins College Publishers: New York, 1993; pp. 650-653.

20. Shriver, D. and P. Atkins, *Inorganic Chemistry*, W.H. Freeman and Company: New York, NY, 1999; pp. 544-546.

21. Buchs, M., C.A. Daul, P.T. Manoharan, and C.W. Schlapfer, *International Journal of Quantum Chemistry* **2003**. 91, 418-431.

22. Coppens, P., I.V. Novozhilova, and A. Kovalevky, *Chemical Reviews* **2002**. 102, 861-883.

23. Enemark, J.H. and R.D. Feltham, *Coordination Chemistry Reviews* **1974**. 13, 339-406.

24. Evans, W. and J.I. Zink, *Journal of the America Chemical Society* **1981**. 103, 2635-2640.

25. Crichton, O. and A.J. Rest, *J Chem Soc Dalton* **1977**. 536-541.

26. Rayner, D.M., A.S. Nazran, M. Drouin, and P.A. Hackett, *Journal of Physical Chemistry* **1986**. 90, 2882-2888.

27. Crichton, O. and A.J. Rest, *Journal of the Chemical Society Dalton Transactions* **1978**. 3, 208-215.

28. Thorsteinson, E.M. and F. Basolo, *Journal of the American Chemical Society* **1966**. 88, 3929-3936.

29. Wang, X.F. and L. Andrews, *Journal of Physical Chemistry A* **2001**. 105, 4403-4409.

30. Kohn, W. and L.J. Sham, *Phys. Rev.* **1965**. 140, A1133.

31. Shao, Y., et al., *Phys. Chem. Chem. Phys.* **2006**. 8, 3172-3191.

32. Becke, A.D., *Physical Review A* **1988**. 38, 3098.

33. Perdew, J.P., *Physical Review B* **1986**. 33, 8822-8824.

34. Niu, S. and M.B. Hall, *Chemistry Reviews* **2000**. 100, 353.

35. The calculated CO stretches of $Co(CO)_3(NO)$ are only 20 cm^{-1} different from the experimental CO stretches.

36. Scott, A.P. and L. Radom, *Journal of Physical Chemistry* **1996**. 100, 16502.

37. Clark, T., J. Chandrasekhar, G.W. Spitvagel, and P.v.R. Schleyer, *Journal of Computational Chemistry* **1983**. 4, 294.

38. Frisch, M.J., J.A. Pople, and J.S. Binkley, *Journal of Chemical Physics* **1984**. 80, 3265.

39. Krishnan, R., J.S. Binkley, R. Seeger, and J.A. Pople, *Journal of Chemical Physics* **1980**. 72, 650.

40. Balabanov, N.B. and K.A. Peterson, *Journal of Chemical Physics* **2005**. 123, 064107.

41. Dunning, T.H.J., *Journal of Chemical Physics* **1989**. 90, 1007-1023.

42. Hay, P.J. and W.R. Wadt, *Journal of Chemical Physics* **1985**. 82, 299-310.

43. Gill, P.M.W., B.G. Johnson, and J.A. Pople, **1993**. 209, 506.

44. Casida, M.E., in *Recent Advances in Density Functional Methods, Part I*, D.P. Chong, Editor. 1995, World Scientific: Singapore.

45. Gross, E.K.U. and W. Kohn, *Adv. Quantum Chem.* **1990**. 21, 255.

46. Petersilka, M., U.J. Gossmann, and E.K.U. Gross, *Physical Review Letters* **1996**. 76,

47. Runge, E. and E.K.U. Gross, *Physical Review Letters* **1984**. 52, 997.

48. Hirata, S. and M. Head-Gordon, *Chemical Physics Letters* **1999**. 291-299.

49. The Maximum Overlap Method is a recently-developed (and unpublished) feature of Q-Chem 3.1, implemented by P. Gill. Originally designed to force oscillating SCF calculations to "choose" a configuration, MOM occupies SCF orbitals by maximum overlap with the previous set of occupied orbitals, instead of the usual occupation of the lowest orbitals. By choosing a configuration in which electrons are promoted to higher orbitals, excited state configurations can be converged, using MOM from the initial SCF guess.

50. Hanlan, L.A., H. Huber, E.P. Kundig, B.R. McGarvey, and G.A. Ozin, *Journal of the America Chemical Society* **1975**. 97, 7054-7068.

51. Bentsen, J.G. and M.S. Wrighton, *J. Am. Chem. Soc.* **1987**. 109, 4518-4530.

52. Glascoe, E.A., M.F. Kling, J.E. Shanoski, and C.B. Harris, *Organometallics* **2006**. 25, 775-784.

53. Grevels, F.W., W.E. Klotzbucher, J. Schrickel, and K. Schaffner, *J. Am. Chem. Soc.* **1994**. 116, 6229-6237.

54. Vergeer, F.W., F. Hartl, P. Matousek, D. Stufkens, and M. Towrie, *Chem. Comm.* **2002**. 1220-1221.

55. DeKock, R.L. and H.B. Gray, *Chemical Structure and Bonding*, University Science Books: Sausilito, CA, 1989; pp. 250-266.

56. Koseki, S., M.W. Schmidt, and M.S. Gordon, *J. Phys. Chem. A* **1988**. 102, 10430.

57. Lengsfield, B.H., J.A. Jafri, and D.H. Phillips, *J. Chem. Phys.* **1981**. 74, 6849.

58. The coordinatively unsaturated singlet was found to bind a solvent molecule, although the nitrosyl bond angle decreased by only 1º and shifted the frequency by 2 cm^{-1}.

59. The CO bond dissociation energy of A was calculated to be 43.0 kcal/mol, easily accessible with a 400 nm photon (ca. 71 kcal/mol). The triplet CO loss intermediate is calculated to be 20.6 kcal/mol above the singlet CO loss intermediate.

60. Based on the absolute DFT calculated frequencies (refer to Table 2), we cannot distinguish between the singlet and triplet forms of $Co(CO)_2(NO)$. However, the DFT calculated frequencies indicate that the NO stretch of the singlet (1803 cm^{-1}) will be higher in energy than the NO stretch of the triplet (1773 cm^{-1}). Thus, we assign the higher energy peak (1775 cm^{-1}) to the singlet $Co(CO)_2(NO)(S)$ and the lower energy peak (1755 cm^{-1}) to the triplet $Co(CO)_2(NO)$

61. The singlet-triplet gap in the singlet geometry is calculated to be 32 kcal/mol.

62. Snee, P.T., C.K. Payne, K.T. Kotz, H. Yang, and C.B. Harris, *Journal of the American Chemical Society* **2001**. 123, 2255-2264.

63. Past studies indicate that triplet coordinatively unsaturated complexes, like $^3Co(CO)_2(NO)$, do not interact strongly with non-polarizable solvents, such as saturated alkanes, and are, therefore, unreactive on a picosecond timescale. DFT calculations confirm these predictions since our attempts to coordinate a hydrocarbon to $^3Co(CO)_2(NO)$ were unsuccessful. On the other hand, $^1Co(CO)_2(NO)$, does coordinate to a saturated hydrocarbon (Figure 9), but our experiments indicate that the singlet-triplet

energy gap is still high enough in solution that the $^3Co(CO)_2(NO)$ to $^1Co(CO)_2(NO)(S)$ spin-crossover reaction does not occur on a picosecond timescale.

64. Yang, H., P.T. Snee, K.T. Kotz, C.K. Payne, and C.B. Harris, *Journal of the American Chemical Society* **2001**. 123, 4204-4210.

65. A full calculation of the ground potential energy surface along the Co-N-O bond angle (0-180^o) is presented in the SI.

66. An eclipsed bent structure, in which the NO bends directly toward a neighboring CO ligand, was found to be a first-order saddle point connecting equivalent minima.

67. The differences in the CO bond parameters are insignificant, and are limited to a minor (<5º) bending of the carbonyl bonds and breaking of symmetry due to the presence of the bent nitrosyl ligand. Additionally, no significant changes were observed in the carbonyl frequencies of the different isomers on the ground or excited potentials.

68. The calcuated barrier to the η^2-S_0 to S_0 isomerization is much smaller than the corresponding barrier for $[Fe(CN)_5(NO)]^{2-}$ (12 kcal/mol).

69. Allen, W.D., Y. Yamaguchi, A.G. Caszar, D.A. Clabo Jr., R.B. Remington, and H.F. Schaefer III, *Chemical Physics* **1990**. 1990, 427-466.

70. Novozhilova, I.V., P. Coppens, J. Lee, G.B. Richter-Addo, and K.A. Bagley, *Journal of the American Chemical Society* **2006**. 128, 2093.

71. We expect that the close approach between S_0 and S_1 enables the formation of η^2 complexes in other transition-metal-NO complexes.

72. Marcus, R.A., *Journal of Chemical Physics* **1956**. 24, 966.

73. Koseki, S., M.W. Schmidt, and M.S. Gordon, *Journal of Physical Chemistry* **1992**. 96, 10768-10772.

74. Walker, T.E.H. and W.G. Richards, *Journal of Chemical Physics* **1970**. 52, 1311-1314.

75. Grampp, G., *Angew. Chem. Int. Ed. Engl.* **1993**. 32, 691-693.

76. Marcus, R.A. and N. Sutin, *Biochim. Biophys. Acta.* **1985**. 811, 265-322.

77. Glascoe, E.A., K.R. Sawyer, J.E. Shanoski, and C.B. Harris, *Journal of Physical Chemistry C* **2007**. 111, 8789-8795.

78. Snee, P.T., C.K. Payne, S.D. Mebane, K.T. Kotz, and C.B. Harris, *Journal of the American Chemical Society* **2001**. 123, 6909.

79. In the plot, S_3 does not show a minimum; along a similar coordinate in which the NO bond angle is the only degree of freedom, a shallow minimum appears as is seen for T_4. This plot may also be found in the SI.

80. Vlcek Jr., A., *Coordination Chemistry Reviews* **2000**. 200, 933-977.

81. While the highest lying triplet state in Figure 11, also has an NO ligand that is less bent than the NO in T_1, we do not expect it to be long-lived. Figure 11 suggests that T_4 will rapidly relax to a lower lying state on a femtosecond timescale.

82. The Co-N-O bond angle in the excited state triplet structures is estimated based on the TD-DFT calculations presented in Figure 11 and is not based on a fully optimized structures.

83. Humprey, W., A. Dalke, and K. Schulten, *J. Molec. Graphics* **1996**. 14, 33-38.

Table 1. Peak assignments and dynamics for the features shown in Figure 4.

Peak	*Species* [a]	*Exp Freq* (cm^{-1})[b]	*τ(ps)*	*Trend*
B	$^3Co(CO)_3(NO)$ (T_2 or T_3)	1715 (NO)	9.4 ± 2	decay
			350 ± 150	decay
		1913 (CO)	5.1 ± 2	rise
			209 ± 78	decay
C	$^3Co(CO)_3(NO)$ (T_1)	1684 (NO)	12 ± 3	decay
			350 ± 100	rise
		1949 (CO)	8.1 ± 3	decay
			297 ± 18	rise
D	$^3Co(CO)_2(NO)$ (T_1)	1755 (NO)	11±1	decay

[a] The electronic state of each species is listed in parentheses. [b] The nature of the stretching modes corresponding to each peak is listed in parentheses. These assignments are based on the frequencies of the modes compared to literature values complexes and the DFT calculations.[4,25,26,29,51]

Table 2. Geometric and energetic parameters of relevant structures, optimized with BP86/6-311+G(3df) (6-31G* on Co).

Electronic State	*Energy (kcal/mol)*	*Bond Length (Å)*				*Bond Angle (deg)*		*Stretching Mode (cm^{-1})*	
		NO	CoN	CO	CoC	CoNO	CoCO	NO	CO
S_0 (**A**)	0.0	1.162	1.661	1.151	1.799 1.800	180.0	178.5[b] 178.4	1842	2015 2016 2076
η^2-S_0	27.9	1.203	1.781	1.150[b] 1.152	1.827 1.781	85.0	174.8[b] 174.9	1510	2011 2014 2070
T_1 (**C**)	38.4	1.184	1.808	1.152[b] 1.151	1.812[b] 1.819	137.1	176.8	1664	1998 2004 2058
$^1Co(CO)_2NO(S)$ (S = ethane)	35.6[d]	1.167	1.641	1.155	1.781	137.1	176.8	1803	1984 2047
S_1	40.4	1.186	1.830	1.182[b] 1.151	1.815[b] 1.817	128.7	178.6[b] 176.5	1659	1998 2040 2067
iso-S_0	42.1	1.161	1.745[a]	1.153	1.792[b] 1.793	179.9[c]	178.0[b] 178.1	1770	1999 2002 2060
$^3Co(CO)_2NO$ (**D**)	56.3[d]	1.177	1.705	1.154	1.804	180.0	180.0	1773	1992 2048

[a] Co-O bond length; [b] geometric parameter for the two identical CO ligands; [c] Co-O-N bond angle; [d] energy including dissociated CO molecule.

Figure 1. Binding modes of a nitrosyl ligand to a transition-metal where the nitrosyl ligands are lying in the same plane as the metal atom. a) Linear M–NO: the σ(NO) orbital is bound to the metal d_{z^2} orbital, and the π^*(NO) orbital participates in π back-bonding with the metal; b) Bent M–NO: the N is sp^2 hybridized and there is a σ-donation between the d_{z^2} orbital on the metal and an sp^2 orbital on the NO. Additionally, there is lone pair on the NO ligand in this geometry. The amount of π back-bonding with the metal center is reduced in this geometry because there is no longer an interaction between the π^*(NO) orbital and the d-orbitals in the plane of the paper; however, there π back-bonding between π^*(NO) orbital and the d-orbitals that are perpendicular to the page ; c) M–ON: identical to the bonding between a metal and a linear NO, except that there is less back-bonding because of the smaller lobes of the oxygen π^* orbitals. d) M–(η^2-NO): the metal is bound in a σ-fashion to the NO bond so that it is oriented in a side-on geometry.[9]

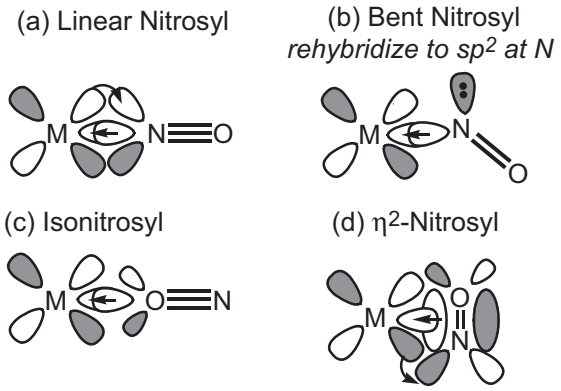

Figure 2. Electronic absorption spectrum of $Co(CO)_3(NO)$ in a neat hexane solution.

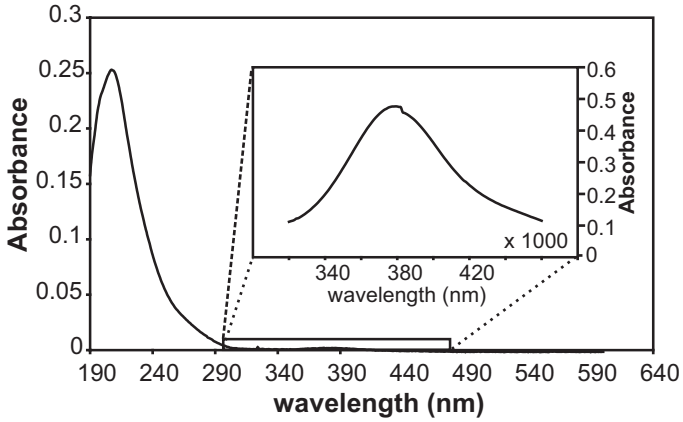

Figure 3. The molecular orbital correlation diagram of the $\{CoNO\}^{10}$ structural unit in the linear-NO and bent-NO forms of $Co(CO)_3(NO)$, predicted by Enemark & Feltham.[23]

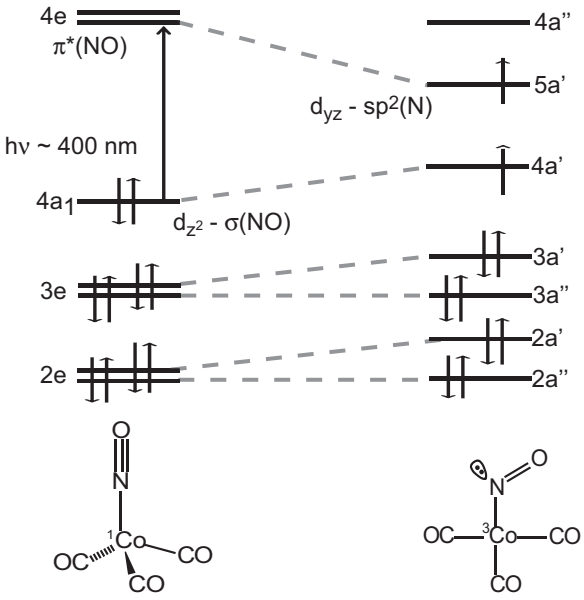

Figure 4. Ultrafast time-resolved visible-pump, mid-IR probe spectra of the (a) NO stretching region of ca. 20 mM $Co(CO)_3(NO)$, (b) NO stretching region of ca. 5 mM $Co(CO)_3(NO)$ and (c) CO stretching region of ca. 5 mM $Co(CO)_3(NO)$ in neat hexane solution. * corresponds to a feature discussed in SI.

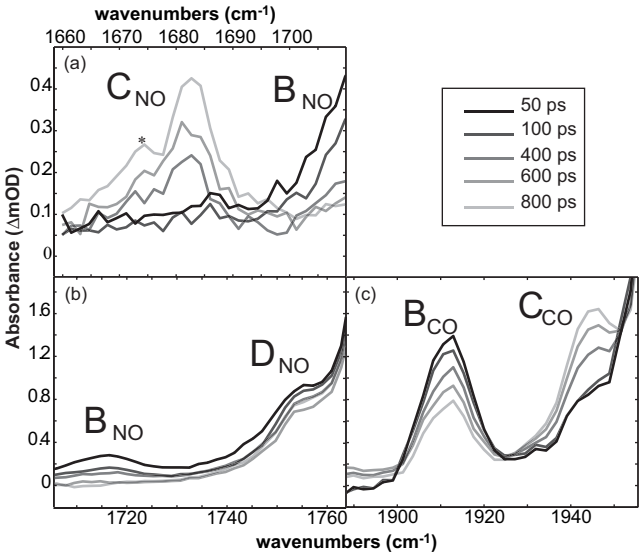

Figure 5. Kinetic plots of the peaks at (a) 1715 cm^{-1} (**B_{NO}**) and (b) 1684 cm^{-1} (**C_{NO}**) in hexane solution.

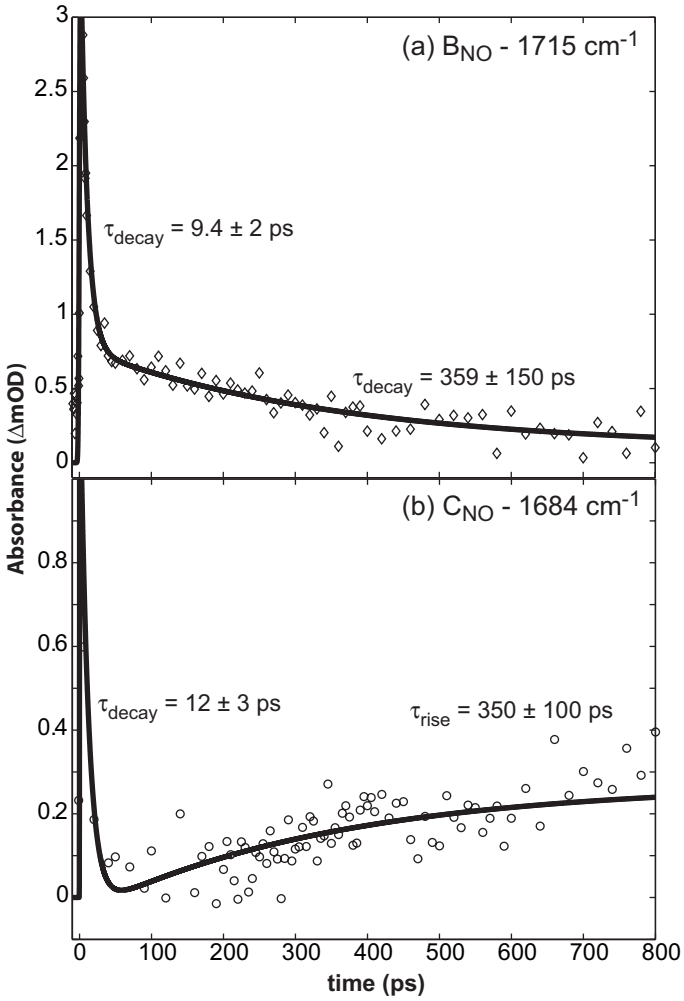

Figure 6. Kinetic plots of the carbonyl stretches of peaks at 1917 cm^{-1} ($\mathbf{B_{CO}}$) and 1949 cm^{-1} ($\mathbf{C_{CO}}$) in solution.

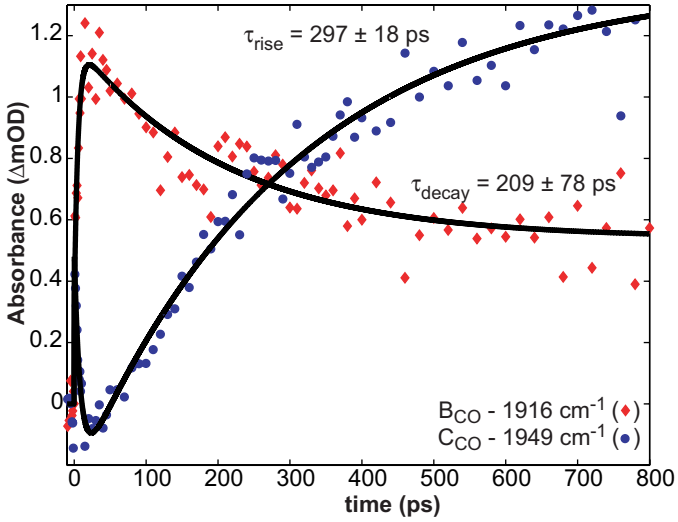

Figure 7. Calculated Kohn-Sham orbital diagram for $Co(CO)_3(NO)$. The analogous diagram for the bent-NO ground state triplet structure is presented in the SI. Plots of orbitals are generated by VMD[83] from Q-Chem outputs. In all cases, the NO is pointing up.

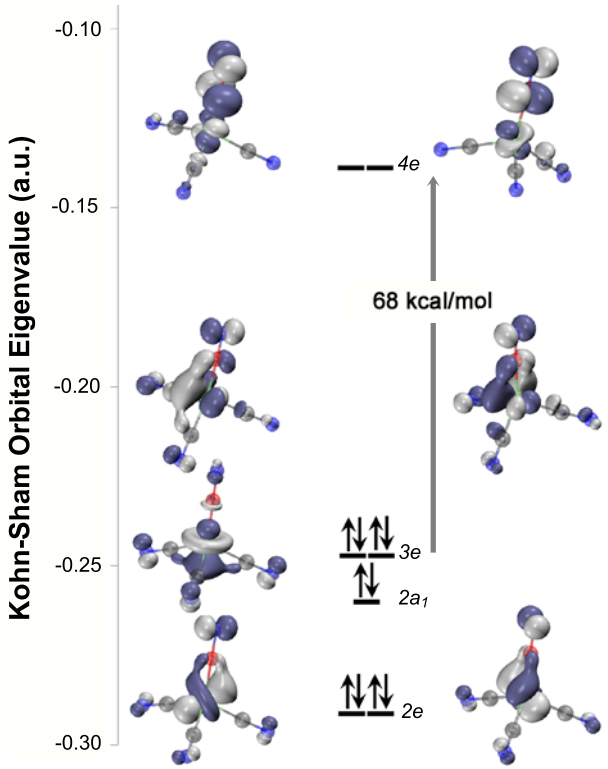

Figure 8. Frontier orbitals (occupied: closed blue circles, unoccupied: open red circles) along the positive half of the NO bending mode (588 cm^{-1}).

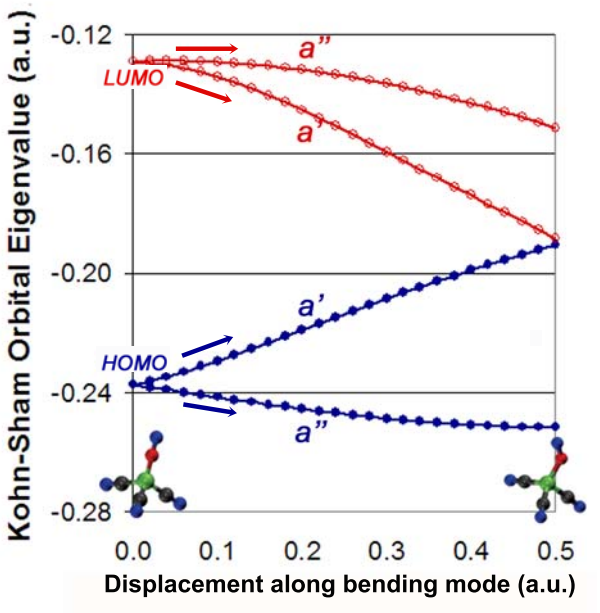

Figure 9. Optimized molecular geometries and harmonic NO stretching frequencies for $Co(CO)_3(NO)$ and the associated CO-loss species.

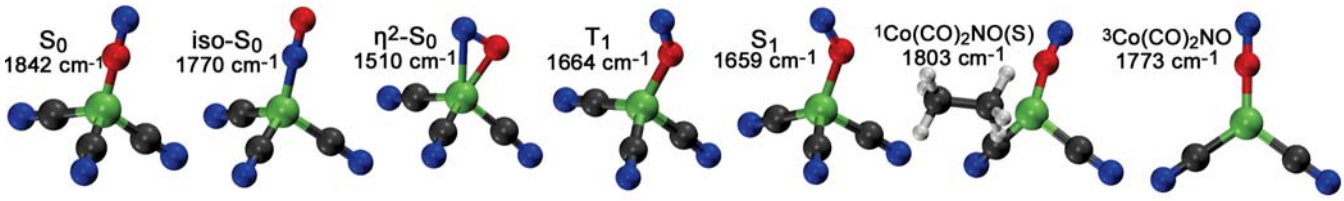

Figure 10. S_0, T_1 and S_1 potential energy surfaces along the Co–N–O bending angle of $Co(CO)_3(NO)$, calculated with BP86/6-31G*: (a) a constrained potential energy scan calculated while fixing the Co–N–O bending angle at successive values ranging between 80º and 180º; (b) single-point energy calculation of S_0^{vert} performed at the optimized structures on the T_1^{opt} state; (c) single-point energy calculation of S_0^{vert} performed at the optimized structures on the S_1^{opt} state The *opt* superscript denotes constrained optimization at a given bending angle. The *vert* superscript signifies a single-point energy calculation on a different potential energy surface, with the same molecular structure as the paired *opt* state.

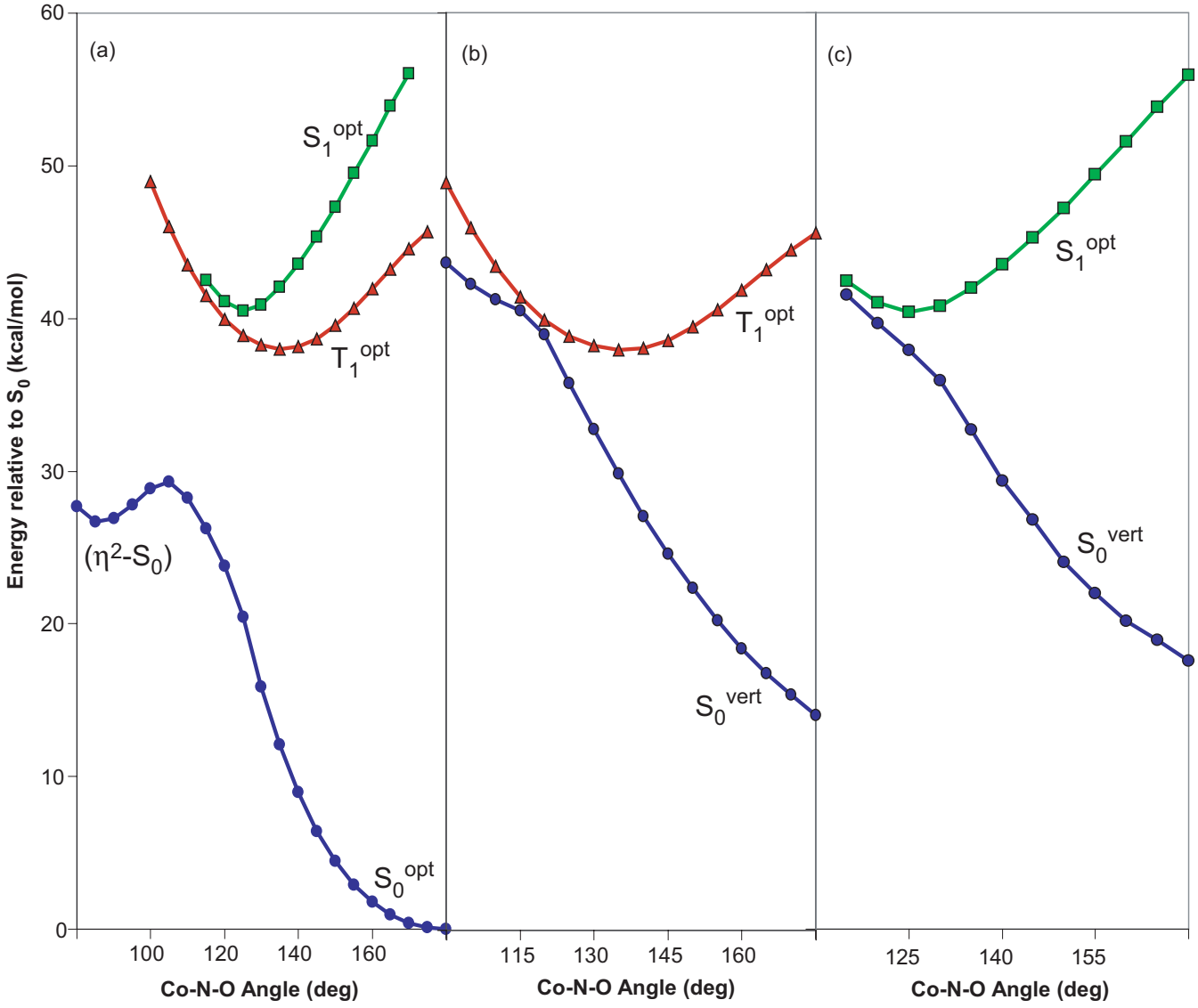

Figure 11. TD-DFT vertical excited states along the bending mode of the parent complex. Shown are the four single-excitation states of each spin symmetry arising from the original doubly degenerate HOMO and LUMO. Singlet states are shown in green (circles), and the triplet states are shown in red (triangles). The symmetries (A' and A'') correspond to the symmetries for the individual states with positive bending modes and the numbering of the states is based on the energy ordering of the states when the complex has a bent-NO geometry. The horizontal dashed line (71 kcal/mol) corresponds to the 400-nm photon energy.

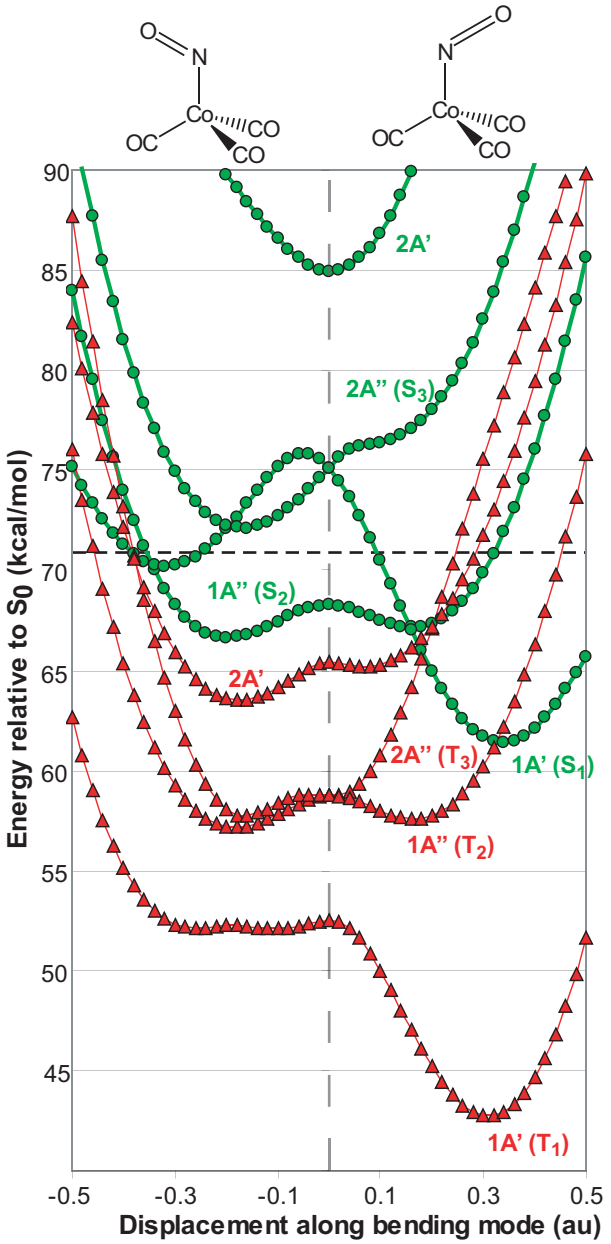

Figure 12. Photochemical mechanism for the formation of excited state bent-NO complexes of $Co(CO)_3(NO)$. While it clear that **B** corresponds to a triplet excited state complex with a bent-NO ligand, we cannot definitively say which state (T_2 or T_3 in Figure 11) is populated.

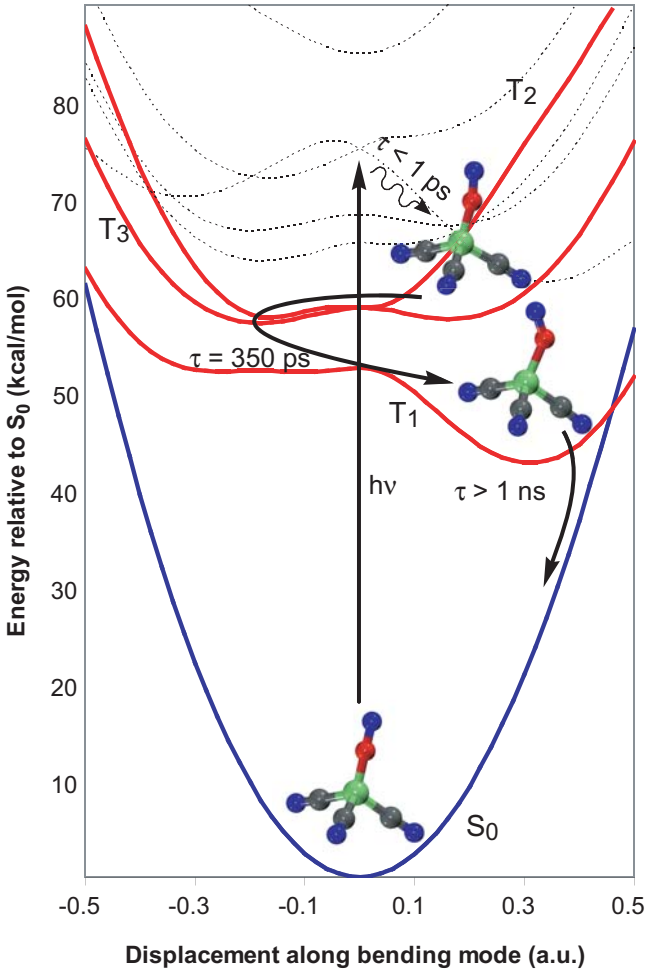

SYNOPSIS TOC